Supporting Information

Direct Electrochemical Functionalization of Graphene Grown on Cu Including the Reaction Rate Dependence on the Cu Facet Type

Minhyeok Kim[†,‡], *Se Hun Joo*[§], *Meihui Wang*[†], *Sergey G. Menabde*[⊥], *Da Luo*[†], *Sunghwan Jin*[†,§], *Hyeongjun Kim*[†,§], *Won Kyung Seong*[†], *Min Seok Jang*[⊥], *Sang Kyu Kwak*[#,*], *Sun Hwa Lee*[†,*], *Rodney S. Ruoff*[†,‡,§,¶,*]

[†]Center for Multidimensional Carbon Materials (CMCM), Institute for Basic Science (IBS), Ulsan, 44919, Republic of Korea

[‡]Department of Chemistry, School of Natural Science, Ulsan National Institute of Science and Technology (UNIST), Ulsan, 44919, Republic of Korea

[§]School of Energy and Chemical Engineering, Ulsan National Institute of Science and Technology (UNIST), Ulsan, 44919, Republic of Korea

[⊥]School of Electrical Engineering, Korea Advanced Institute of Science and Technology (KAIST), Daejeon, 34141, Republic of Korea.

[#]Department of Chemical and Biological Engineering, Korea University, Seoul, 02841, Republic of Korea

[¶]Department of Materials Science and Engineering, Ulsan National Institute of Science and Technology (UNIST), Ulsan, 44919, Republic of Korea

Corresponding authors:
Sang Kyu Kwak, Email: skkwak@korea.ac.kr
Sun Hwa Lee, Email: sunhwa.lee82@gmail.com or sunhlee@ibs.re.kr
Rodney S. Ruoff, Email: ruofflab@gmail.com or rsruoff@ibs.re.kr

Table of Contents

Figure S20. Optimized structure of neutral and reduced 4-iodoaniline with molecular orbital energy levels and spin density.

Figure S21. Gr/Cu(111) and Gr/Cu(115) slab models with aniline adsorbed at symmetrically inequivalent adsorption sites.

Figure S22. Energy diagram for the functionalization of 4-iodoaniline on Gr/Cu(111) and Gr/Cu(115) surfaces.

Figure S1. Photograph of the electrochemical cell after reaction at -2.06 V and room temperature for 10 min.

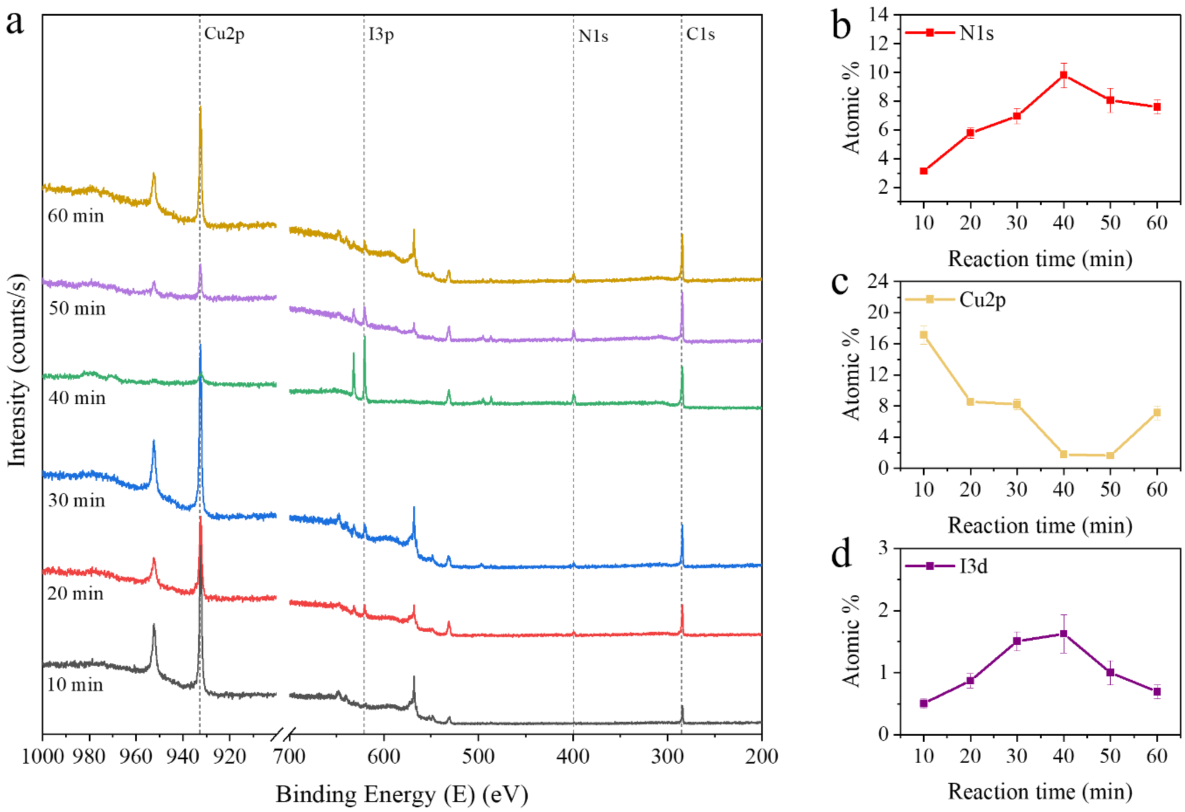

Figure S2. (a) XPS survey spectra of the graphene reacted for 10, 20, 30, 40, 50, and 60 min. Atomic percentage (at%) of (b) N from N1s, (c) Cu from Cu2p, and (d) I from I3d, presented as the average of different spectra measured from eight different and equally spaced locations—from one edge of the sample to the other.

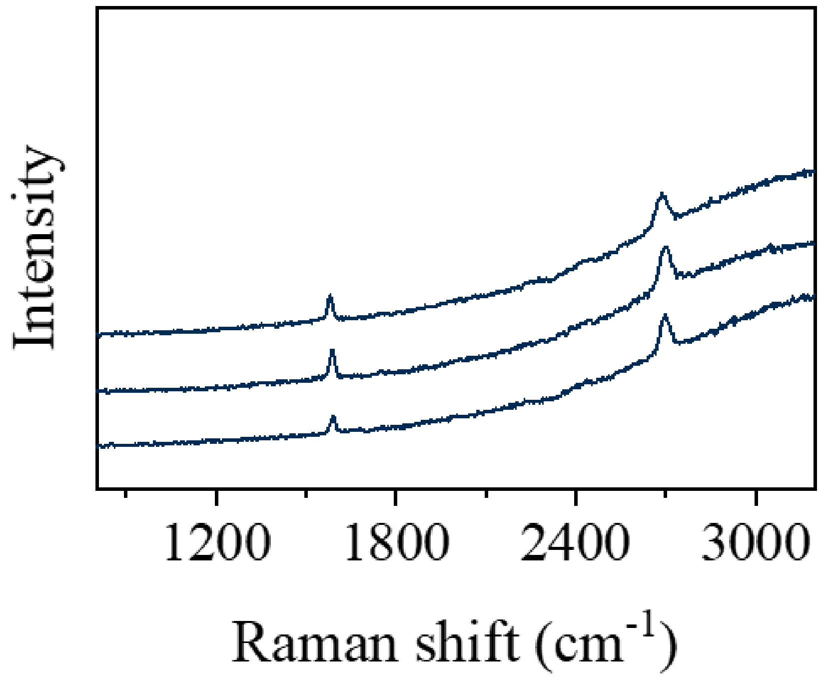

Figure S3. Raman spectra of graphene that was under the same electrochemical reaction condition for 30 min at -2.06 V in a solution composed of $TBAPF_6$ (0.50 M) without 4-iodoaniline. The 3 points were randomly chosen.

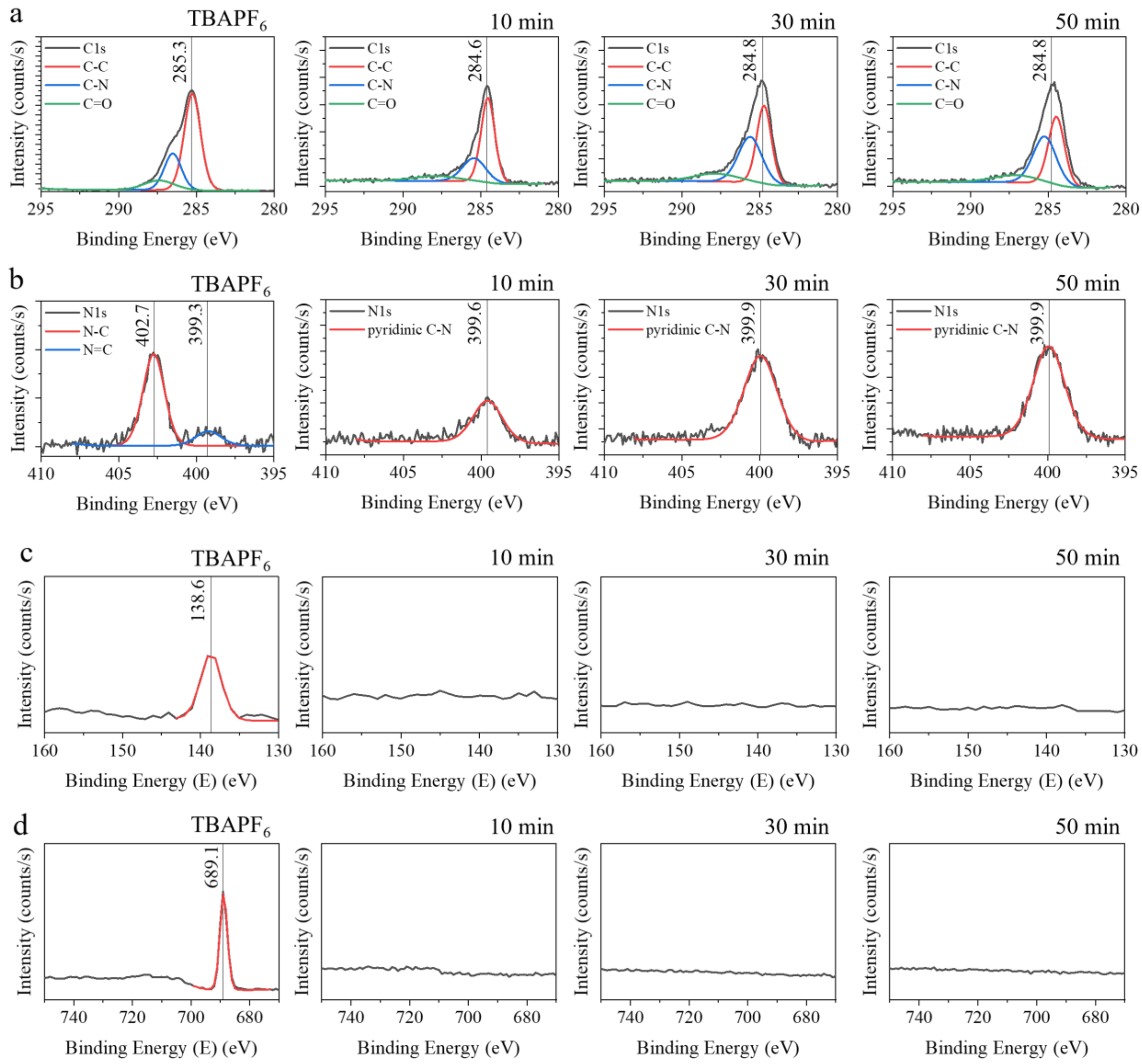

Figure S4. (a) C1s, (b) N1s, (c) P2p, and (d) F1s XPS spectra of $TBAPF_6$ that was dissolved in acetonitrile and deposited on Cu foil, after graphene had been reacted for 10 min, 30 min, and 50 min, using these reaction conditions: -2.06 V was applied in a solution of 4-iodoaniline (15 mM) and $TBAPF_6$ (0.50 M). The reacted graphene samples were washed with acetone, prior to the deposition of the $TBAPF_6$.

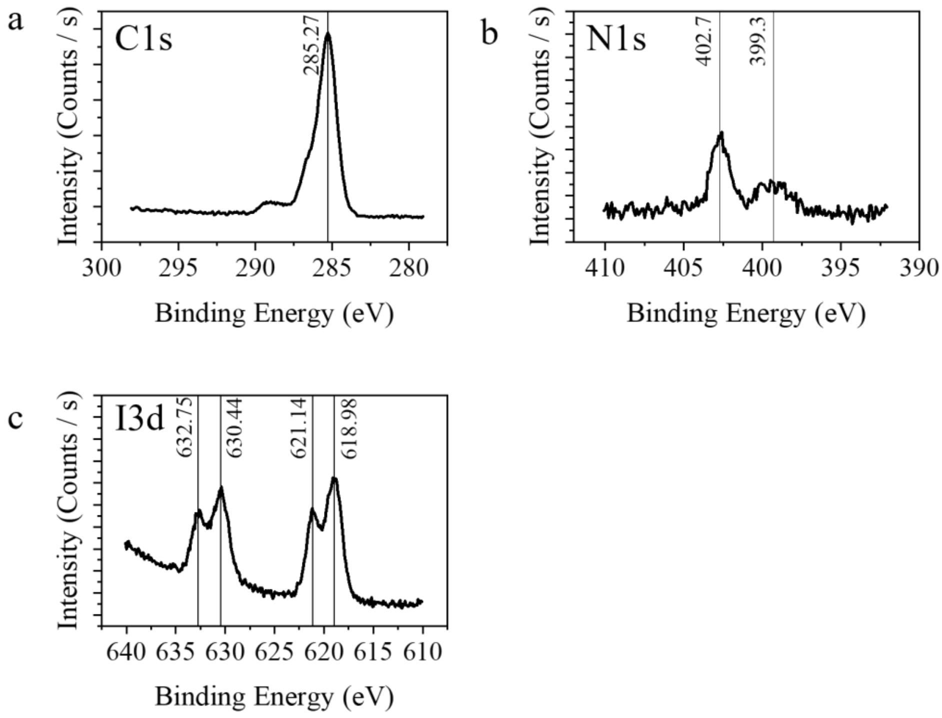

Figure S5. (a) C1s, (b) N1s, and (c) I3d XPS spectra of 4-iodoaniline. The sample was prepared by depositing the 4-iodoaniline that was dissolved in acetonitrile (15 mM) onto Cu(111) foil.

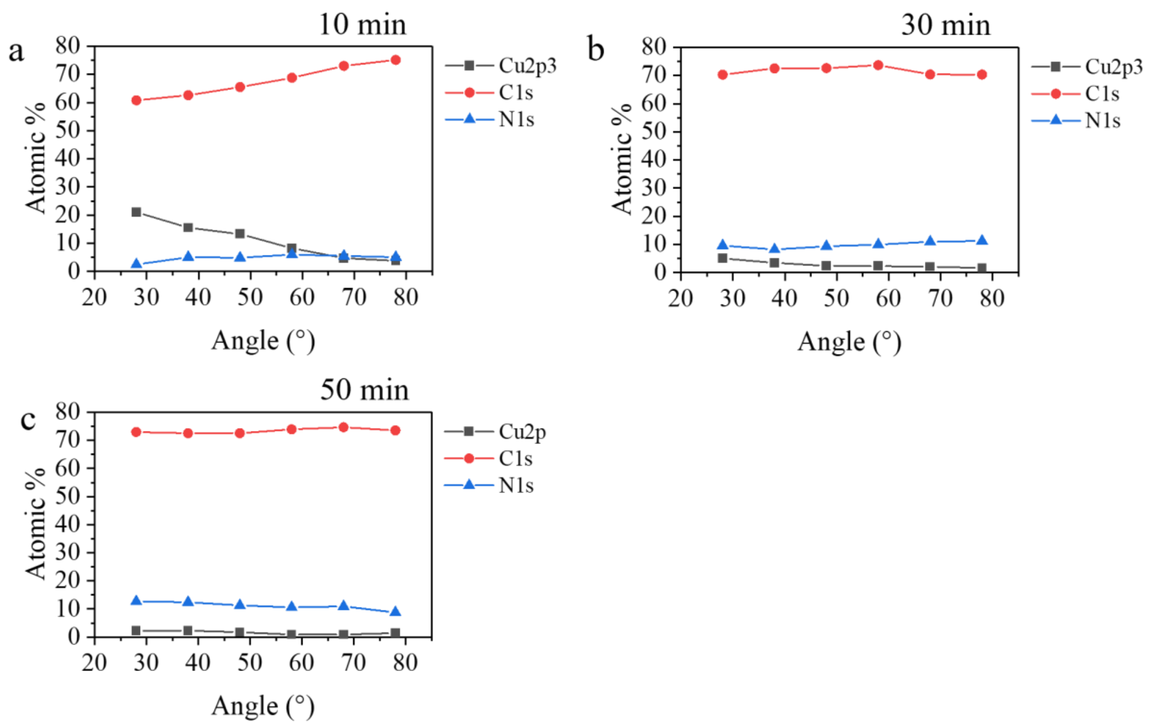

Figure S6. Atomic percentages of C, N, and Cu, from C1s, N1s, and Cu2p spectral regions measured using angle-resolved XPS. The graphene that was reacted for (a) 10 min, (b) 30 min, and (c) 50 min were measured at angles varying from 28° to 78°. These graphene samples were reacted at -2.06 V in a solution of 4-iodoaniline (15 mM) and $TBAPF_6$ (0.50 M).

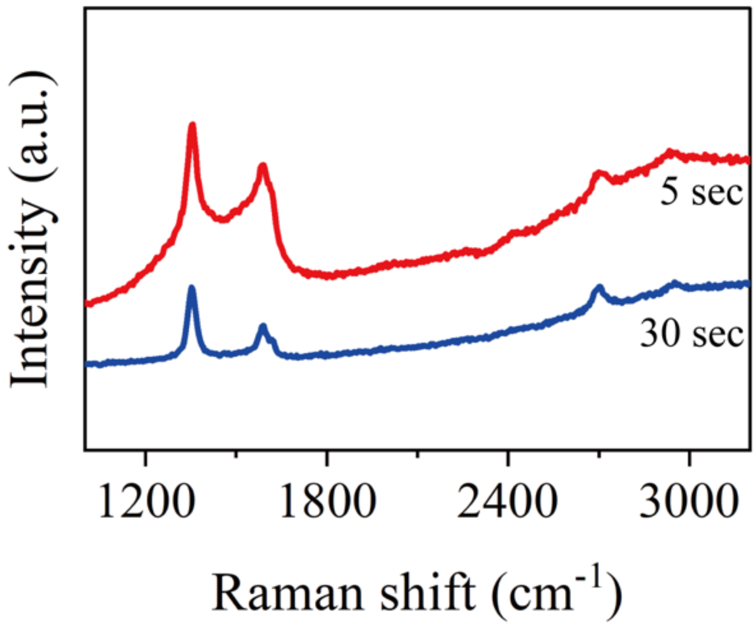

Figure S7. Raman spectra of graphene reacted for 50 min with 4-iodoaniline. Both spectra were measured at the same position with an incident laser of λ = 488 nm. The exposure times for the red and blue lines were 5 s and 30 s, respectively.

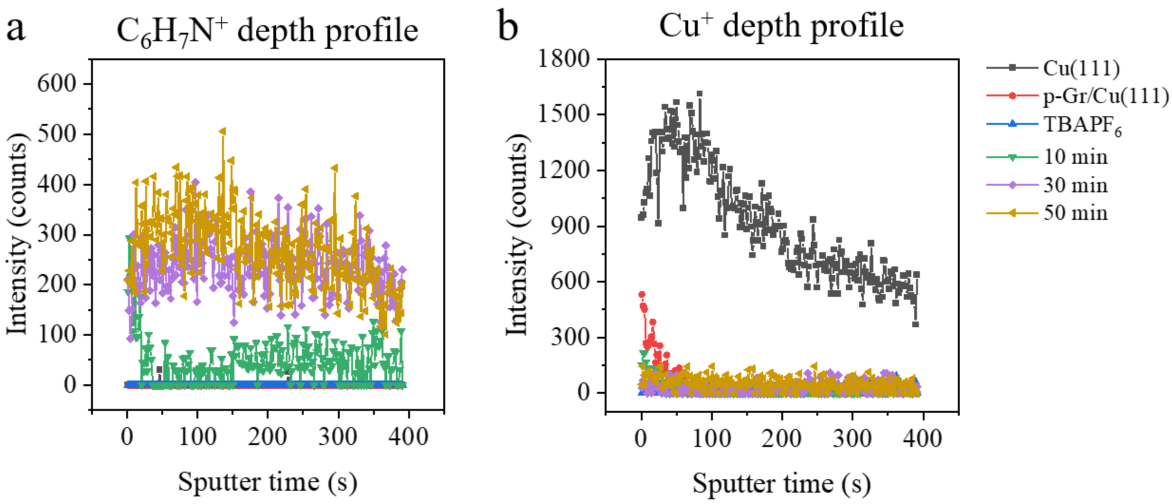

Figure S8. Orbitrap SIMS depth profile of (a) $C_6H_7N^+$ (m/z 93.057) and (b) Cu^+ (m/z 62.929) measured on bare Cu(111), pristine graphene on Cu(111) (p-Gr/Cu(111)), graphene sample reacted for 30 min in a $TBAPF_6$ solution (0.50M) in acetonitrile, and graphene reacted for 10, 30, and 50 min in a reaction solution containing 4-iodoaniline (15 mM) and $TBAPF_6$ (0.50M). The samples were sputtered and analyzed with a 5 keV Ar cluster ion beam.

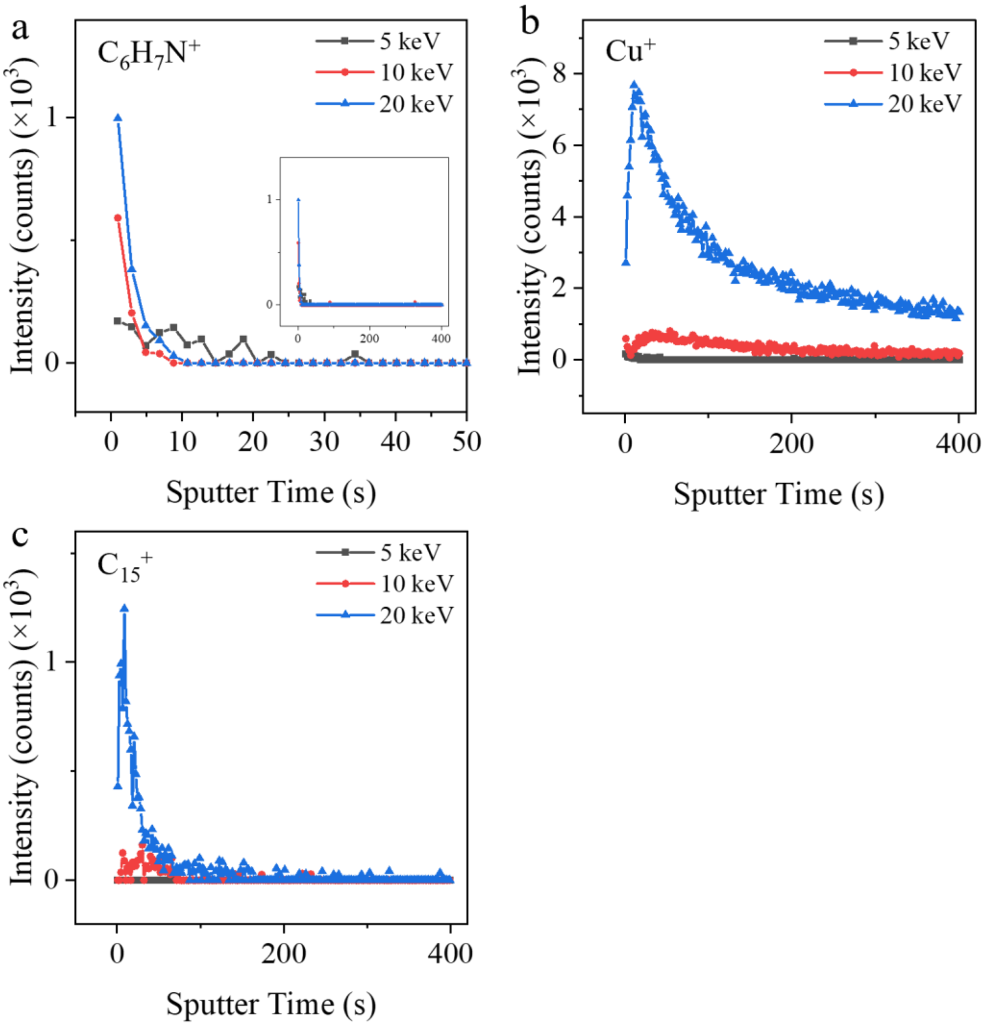

Figure S9. Orbitrap SIMS depth profile of (a) $C_6H_7N^+$ (m/z 93.057), (b) Cu^+ (m/z 62.929), and (c) C_{15}^+ (m/z 179.999) measured on the graphene sample dipped in liquid aniline (99.5%) for an hour and washed with acetone. The inset of (a) shows the depth profile with the extended sputter time to 400 s. The samples were sputtered and analyzed with different Ar cluster ion beam kinetic energies: 5 keV, 10 keV, and 20 keV.

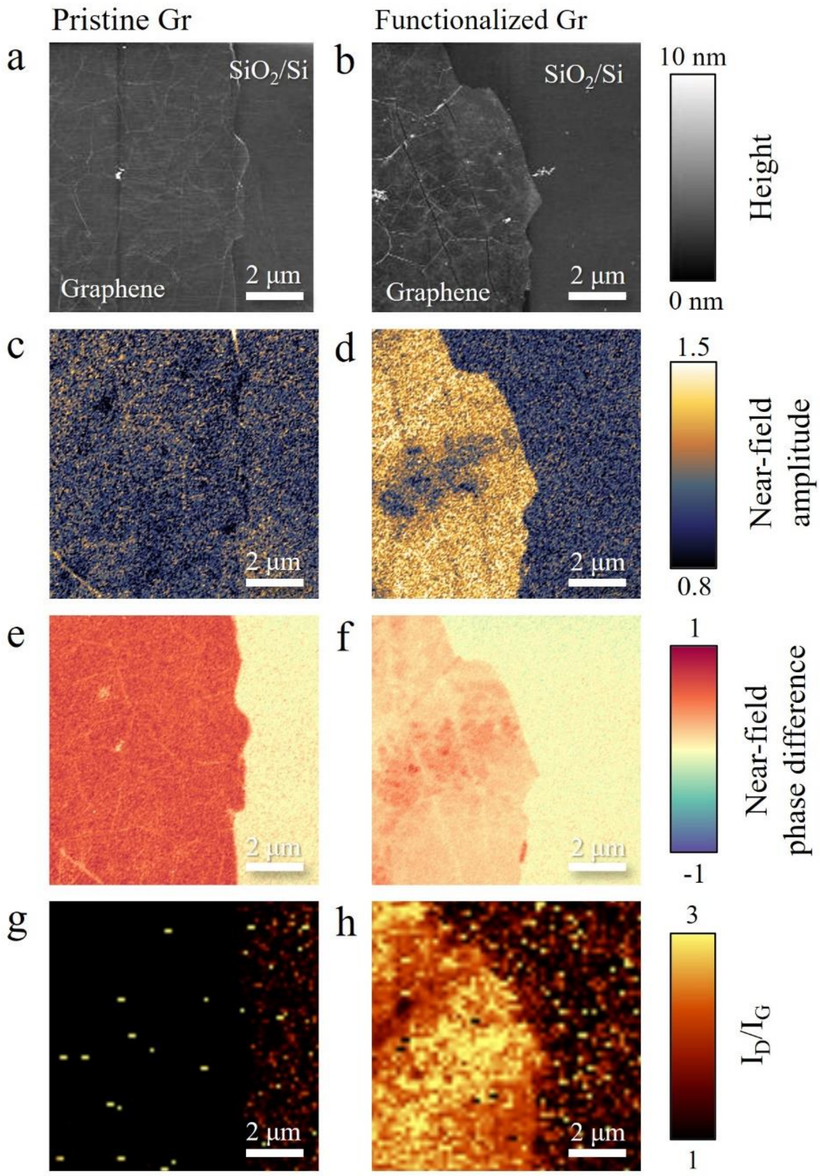

Figure S10. Scattering-type scanning near-field optical microscope (s-SNOM) measurements. (a, b) AFM height maps, (c, d) near-field amplitude maps normalized by the signal over SiO_2 substrate, (e, f) and near-field phase difference maps (in π) of pristine graphene (e) and functionalized graphene (f) that were transferred onto SiO_2/Si substrate. The wavelength of the excitation laser was $\lambda = 6.18$ µm ($\omega = 1619$ cm^{-1}). (g, h) I_D/I_G maps were measured on the corresponding region by Raman spectroscopy with a laser $\lambda = 488$ nm. The functionalized graphene was prepared by applying -2.1 V for 5 min in the solution made of 0.5 M of $TBAPF_6$ and 30 mM of 4-iodoaniline in acetonitrile.

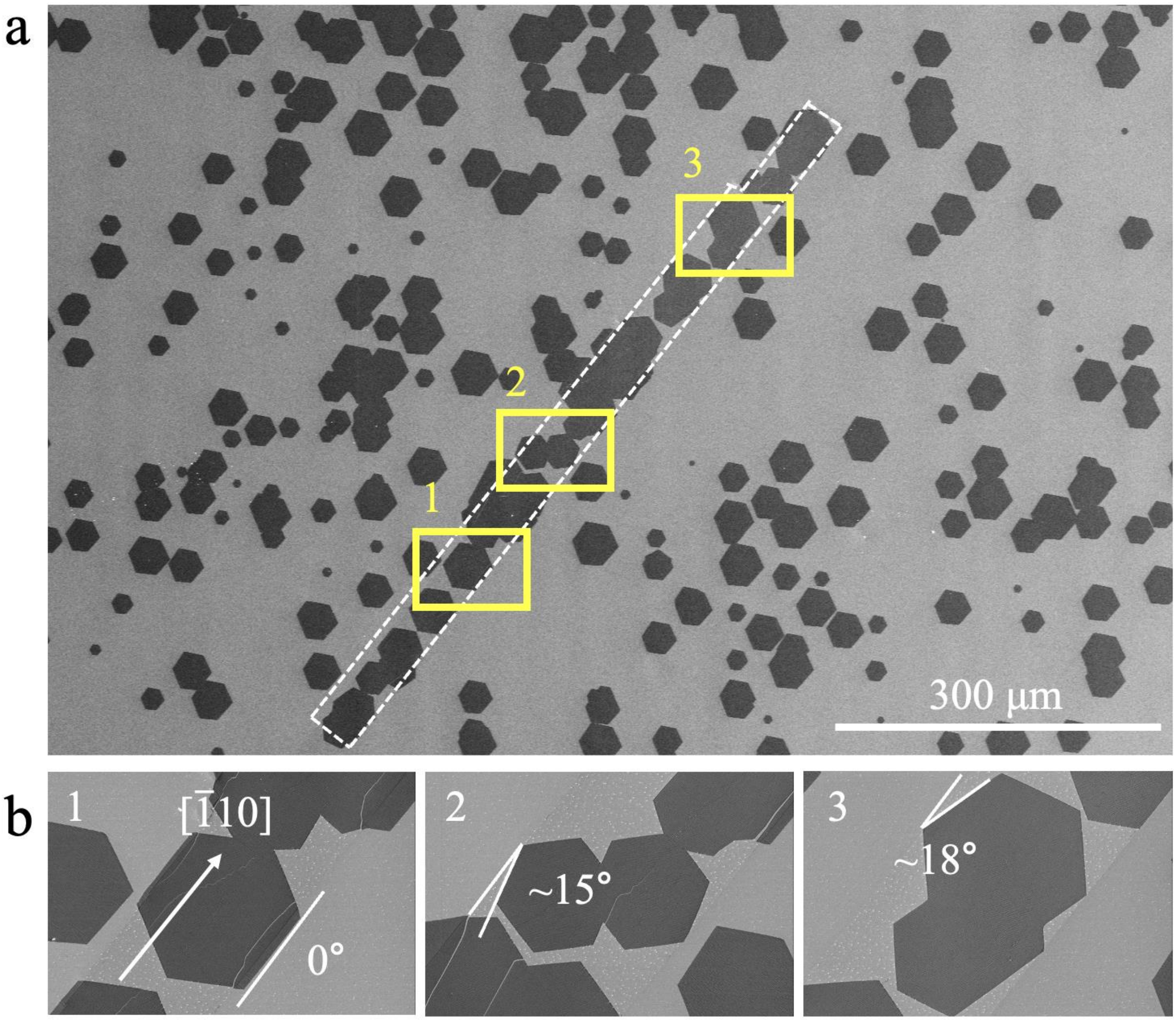

Figure S11. (a) Scanning electron microscopy (SEM) image of graphene islands on Cu (111) including a long rectangular Cu (115) facet indicated by the white dashed line. The numbers 1, 2, and 3 in (a) indicate different orientations of the graphene islands and (b) is a magnified image of the graphene islands. The orientation of (b1) is the dominant orientation of graphene island edges on Cu(115), which has its edge parallel to the [$\bar{1}$10] direction of Cu. Two different orientations of graphene islands are shown in b2 and b3.

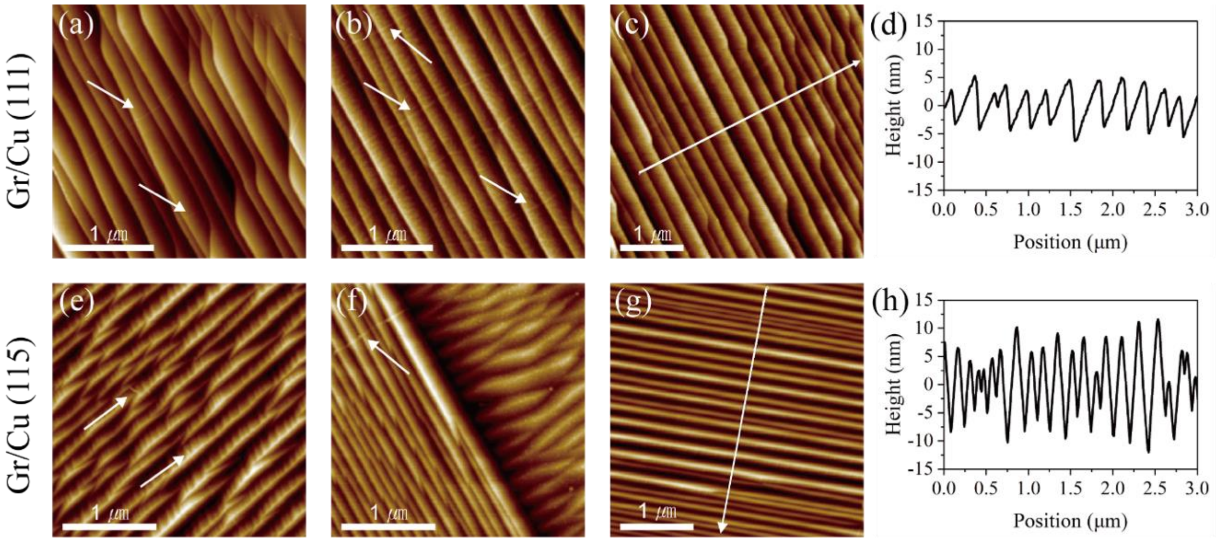

Figure S12. AFM height maps of graphene on Cu(111) and Cu(115). The white arrows indicate ripples on (a, b) Gr/Cu(111) and (e, f) Gr/Cu(115). Height profiles of graphene perpendicular to the step edge on (d) Gr/Cu(111) and (h) Gr/Cu(115); the corresponding lines are indicated on AFM images (c) and (g) by long white arrows.

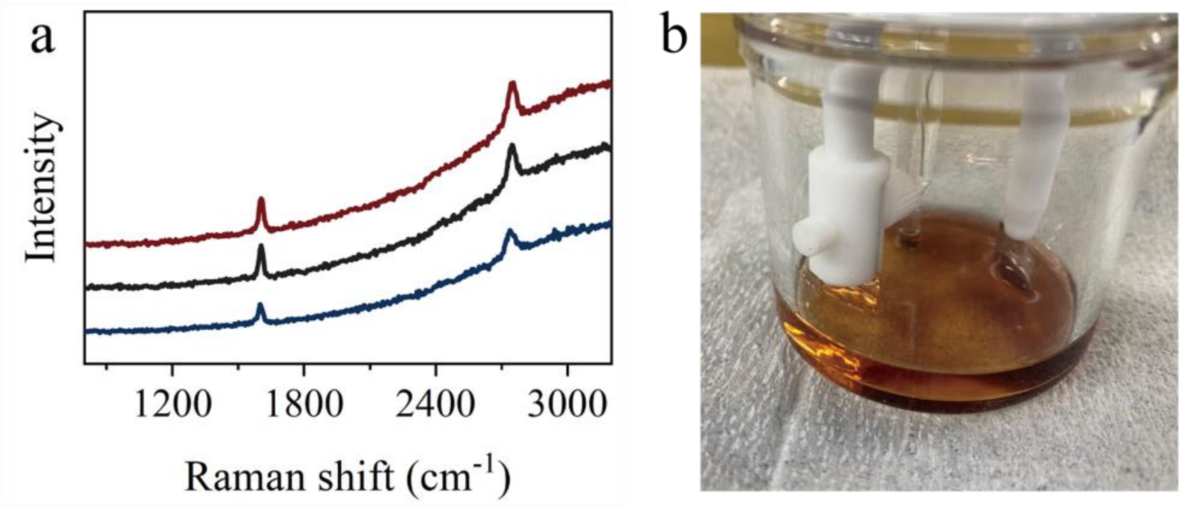

Figure S13. (a) Raman spectra of the graphene reacted for 30 min at -1.70 V (vs. Ag/$AgNO_3$) in a solution of 4-iodoaniline (15 mM) and $TBAPF_6$ (0.50 M) in acetonitrile. Three random positions were chosen. (b) Photograph of the reaction solution exhibiting a color change after the reaction.

Computational Details

Density functional theory calculation

Spin-polarized density functional theory (DFT) calculations were performed using the Vienna Ab initio Simulation Package (VASP) within the projector-augmented wave (PAW) scheme.[1,2] The generalized gradient approximation (GGA) with the Perdew–Burke–Ernzerhof (PBE) functional was used for the exchange correlation functionals.[3] The long-range van der Waals interactions were corrected using Grimme's D2 method.[4] An energy cutoff of 550 eV was defined for the plane-wave basis set. Dipole correction was applied along the out-of-surface direction. The convergence criterion for the electronic self-consistent field calculations was set to 1×10^{-6} eV. Geometry optimization was performed until the Hellmann–Feynman forces were less than 0.01 eV/Å. The Brillouin zone was integrated using gamma-centered k-point grids: 8 × 8 × 8 for the Cu bulk, 3 × 3 × 1 for Cu(111) and Gr/Cu(111), and 2 × 3 × 1 for Cu(115) and Gr/Cu(115). Denser k-point meshes were used for the work function calculations: 12 × 12 × 1 for Cu(111) and Gr/Cu(111), and 8 × 12 × 1 for Cu(115) and Gr/Cu(115).

The Cu(111) and Cu(115) surfaces were modeled as slab models of four atomic layers based on the optimized Cu bulk structure (Figure S14). A vacuum slab was added by adjusting the lattice parameter to 35 Å. The atomic positions of the bottom-most Cu layer were fixed throughout all calculations. For the relaxed Cu(111) and Cu(115) slab models, the surface energies (γ) were calculated using the following equation:

$$\gamma = (E_{\mathrm{slab}} - n \times E_{\mathrm{bulk}})/2A,$$

where E_{slab} is the total energy of the Cu slab, E_{bulk} is the energy per atom of the Cu bulk, n is the total number of atoms in the Cu slab, and A is the surface area of the Cu slab. Based on the results of the Monte Carlo simulations (Figures S15 and S16), Gr/Cu(111) and Gr/Cu(115) were modeled by considering various stacking configurations of graphene (Figure S17). For the optimized Gr/Cu(111) and Gr/Cu(115) structures, the binding energy (E_{b}) of graphene on the Cu surface was calculated using the following equation:

$$E_{\mathrm{b}} = (E_{\mathrm{Gr/Cu}} - E_{\mathrm{Gr}} - E_{\mathrm{Cu}})/A,$$

where $E_{\mathrm{Gr/Cu}}$ is the total energy of the graphene adsorbed on the Cu surface, E_{Gr} is the energy of the graphene, E_{Cu} is the energy of the Cu slab, and A is the surface area of the Cu slab. The work functions (Φ) of the Cu and Gr/Cu models were calculated using the following equation:

$$\Phi = E_{\mathrm{VAC}} - E_{\mathrm{F}}$$

where E_{VAC} is the vacuum level, and E_{F} is the Fermi level of each slab model. The adsorption energy (E_{ad}) of 4-iodoaniline on the Gr/Cu surface was calculated using the following equation:

$$E_{\mathrm{ad}} = (E_{\mathrm{A-Gr/Cu}} + E_{\mathrm{I_2}}) - (E_{\mathrm{I-A}} - E_{\mathrm{Gr/Cu}}),$$

where $E_{\mathrm{A-Gr/Cu}}$, $E_{\mathrm{I_2}}$, $E_{\mathrm{I-A}}$, and $E_{\mathrm{Gr/Cu}}$ are the energies of the aniline-adsorbed Gr/Cu, iodine in the solid state, isolated 4-iodoaniline molecule, and pristine Gr/Cu model, respectively.

Monte Carlo simulations

To investigate the energetically stable orientations and stacking structures of graphene on the Cu(111) and Cu(115) surfaces, Monte Carlo (MC) simulations were performed using the Adsorption Locator module in Materials Studio 2019.[5] The unit cell for the Cu(111) and Cu(115) surfaces was modeled as a slab of nine atomic layers based on the optimized crystal structure of Cu metal. To minimize spurious interactions between the periodic structures in the direction normal to the surface, a 50-Å-thick vacuum slab was added along the out-of-surface direction. A 23 × 40 supercell for Cu(111) and an 8 × 40 supercell for Cu(115) were then constructed to model surfaces with dimensions of approximately 10 nm × 10 nm, which were sufficiently large to simulate a graphene nanoflake of approximately 6 nm with a hexagonal shape (Figures S15 and S16). The interactions between the graphene and Cu surface were described using the COMPASS II force field.[6] The van der Waals interactions were calculated with a cutoff distance of 12.5 Å, and the electrostatic interactions were calculated using the Ewald summation method.[7] For each surface, MC simulations were performed using the Metropolis algorithm and the simulated annealing method. The number of temperature cycles was set to three, and the number of MC steps for each temperature cycle was 1.5×10^4. For 1000 low-energy configurations, geometry optimization was performed until the convergence criteria were satisfied: 2.0×10^5 kcal/mol for the energy change, 0.001 kcal/mol/Å for the maximum force, and 1.0×10^5 for the maximum displacement.

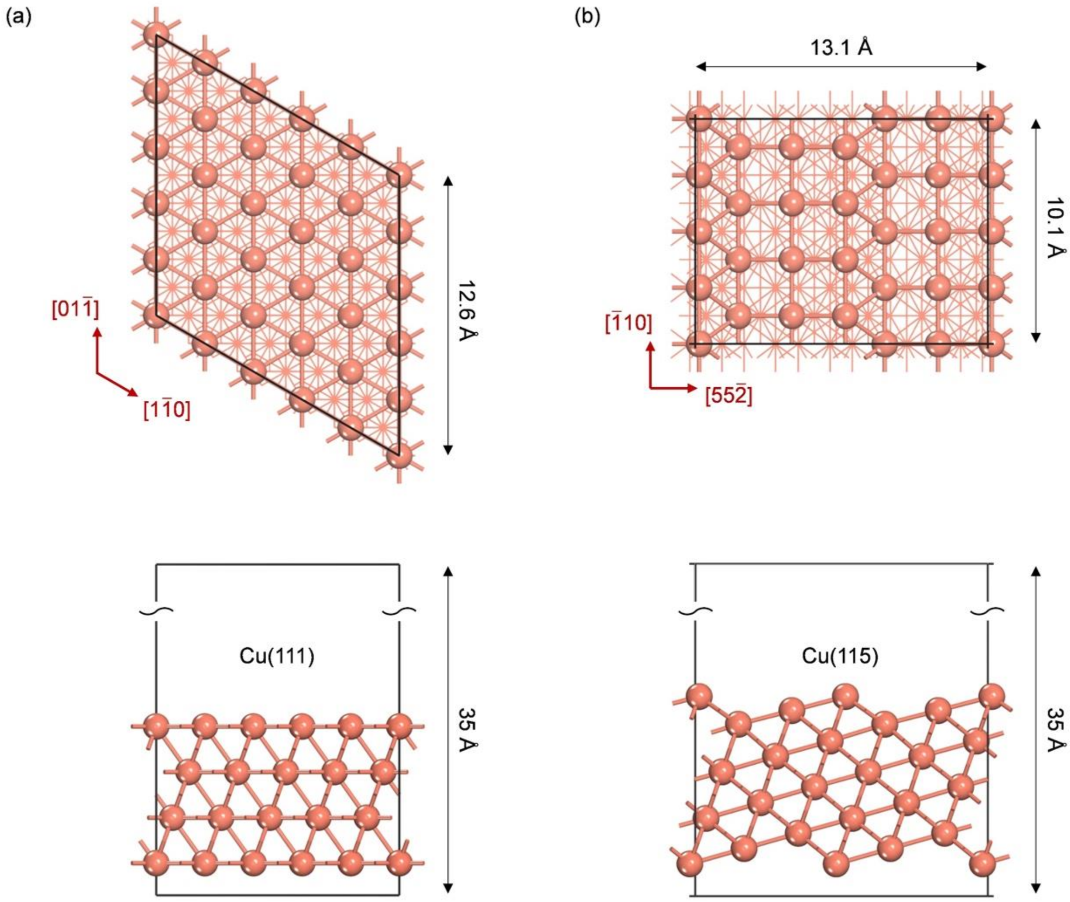

Figure S14. Slab models of (a) Cu(111) and (b) Cu(115) surfaces for DFT calculations (top: top view, bottom: side view). In the top view, only the topmost Cu atomic layer is shown as a ball-and-stick model for clarity.

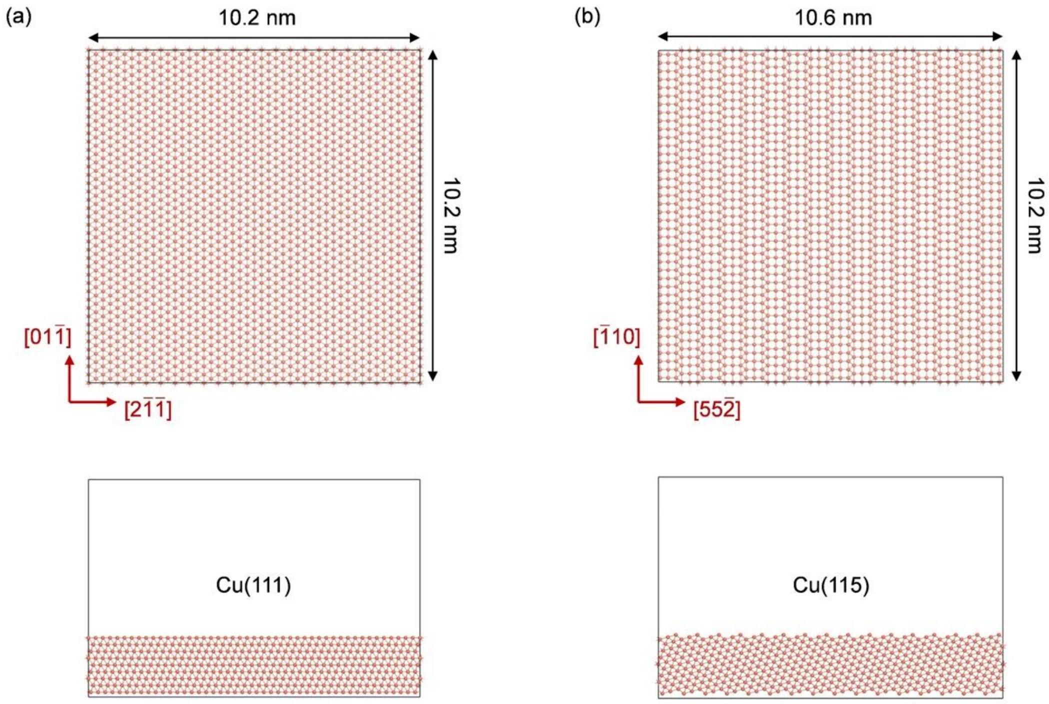

Figure S15. Slab models of (a) Cu(111) and (b) Cu(115) surfaces for MC simulations (top: top view, bottom: side view). In the top view, only the topmost Cu atomic layer is shown as a ball-and-stick model for clarity.

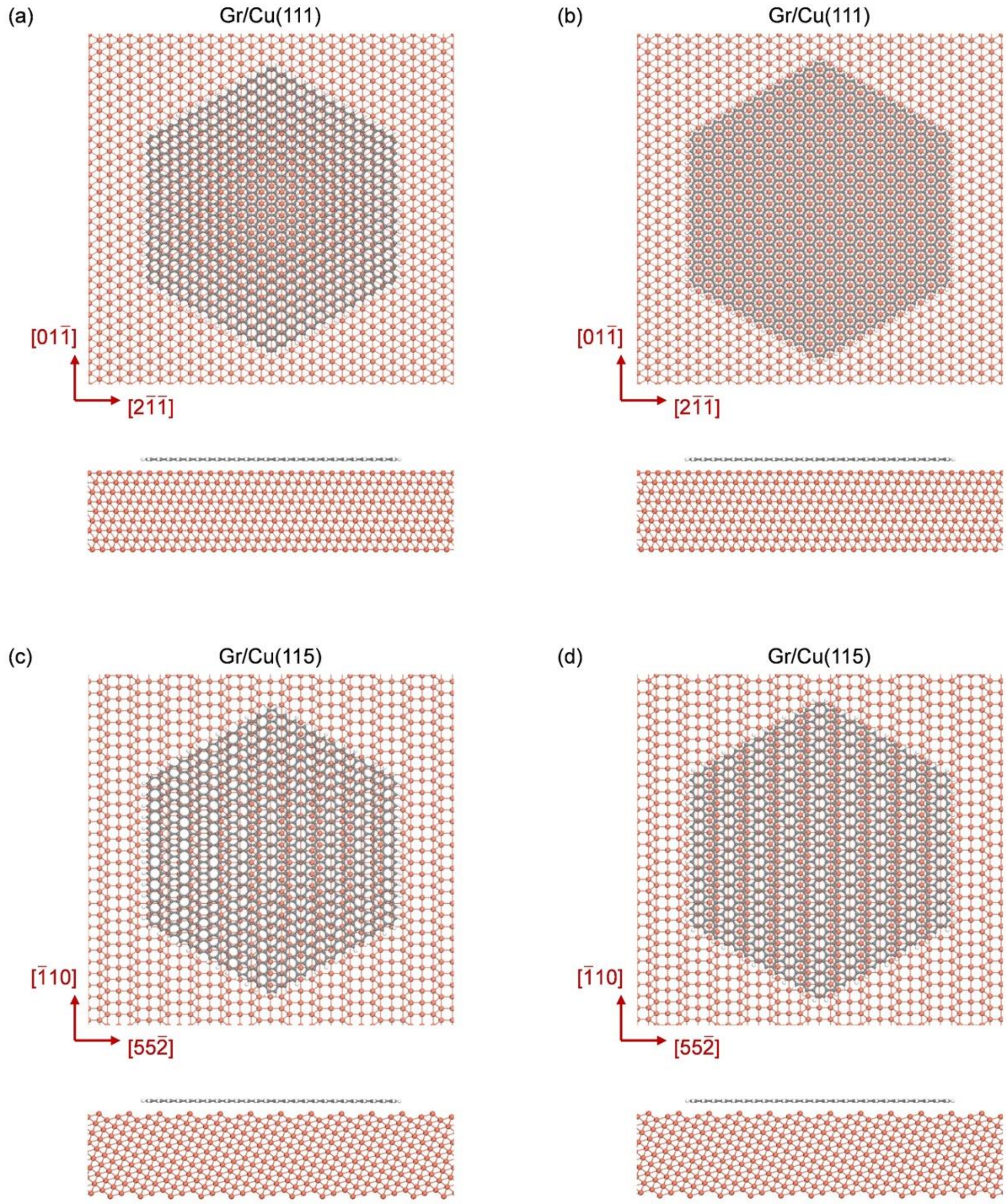

Figure S16. Energetically preferred orientations of graphene islands on the Cu surface (top: top view, bottom: side view). (a, b) The most stable orientation of graphene island on the Cu(111) surface for (a) pristine graphene and (b) graphene with 3.9% tensile strain. (c, d) The most stable orientation of graphene island on the Cu(115) surface for (c) pristine graphene and (d) graphene with 3.9% tensile strain. The lattice parameter of graphene with a tensile strain is 2.56 Å (2.46 Å for pristine graphene), which is the same as that of the Cu substrate.

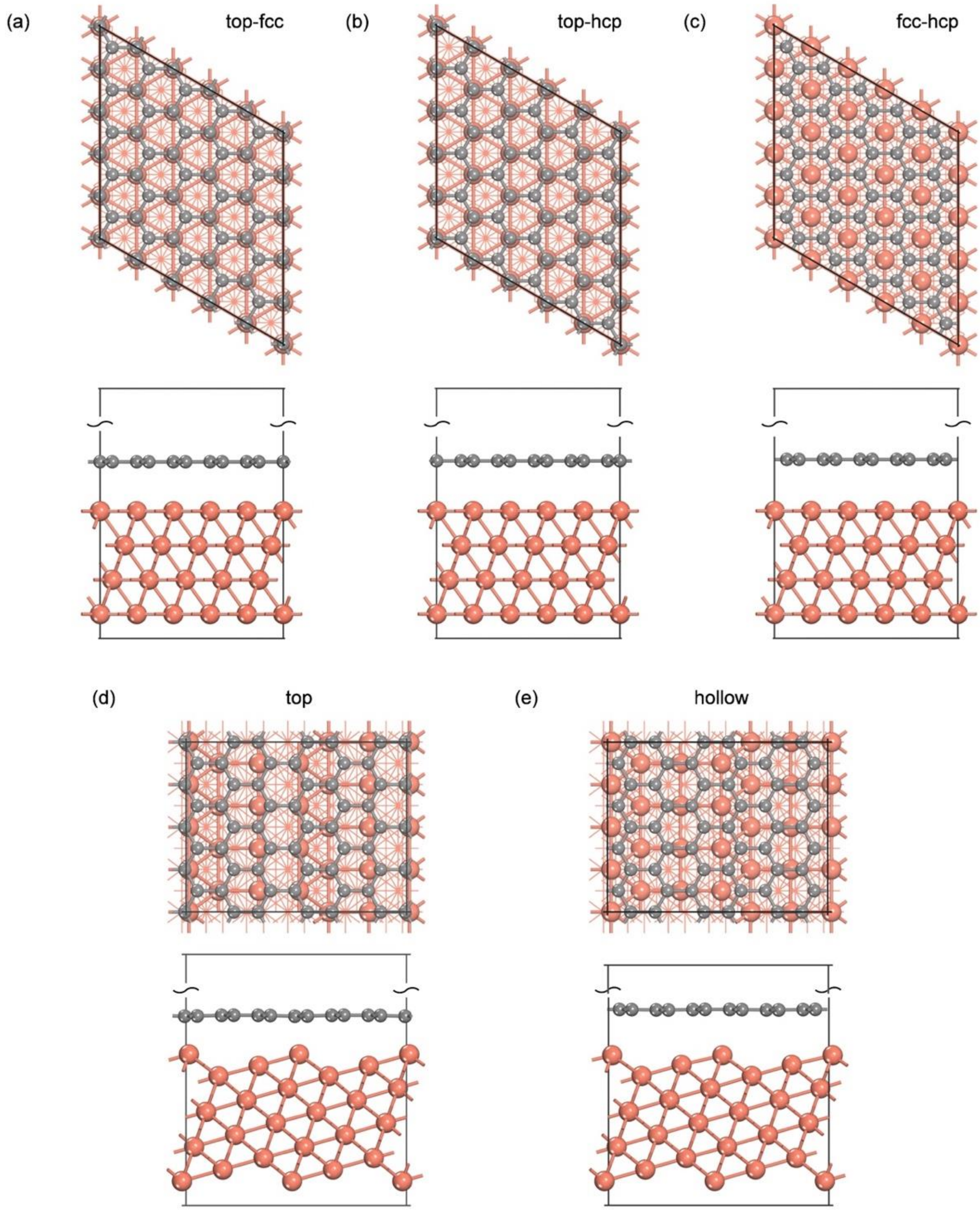

Figure S17. Various stacking configurations of graphene on the Cu surface (top: top view, bottom: side view). (a–c) Three stacking configurations of graphene on the Cu(111) surface: (a) top-fcc, (b) top-hcp, and (c) fcc-hcp. (d, e) Two stacking configurations of graphene on the Cu(115) surface: (d) top and (e) hollow. In the top view, only the topmost Cu layer is shown as a ball-and-stick model for clarity.

Table S1. Binding energy (E_b) of graphene on the Cu surface and the shortest perpendicular distance ($d_\perp$) between graphene and the Cu surface for various stacking configurations of graphene on the Cu(111) and Cu(115) surfaces.

System	Stacking configuration	E_b (J/m^2)	$d_\perp$ (Å)
Gr/Cu(111)	top-fcc	-0.593	2.95
	top-hcp	-0.579	2.99
	fcc-hcp	-0.522	3.07
Gr/Cu(115)	top	-0.599	2.27
	hollow	-0.512	2.70

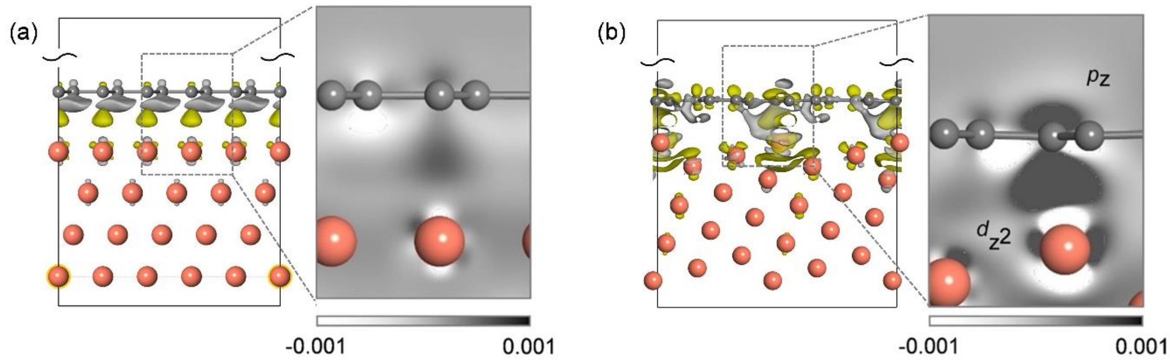

Figure S18. Charge density difference induced by the adsorption of graphene on the Cu surface for (a) Gr/Cu(111) and (b) Gr/Cu(115). Charge density differences were obtained by subtracting the total charge of the system from the individual charges of the Cu slab and the graphene as follows: $\Delta\rho_{Gr/Cu} = \rho_{Gr/Cu} - (\rho_{Gr} + \rho_{Cu})$, where $\rho_{Gr/Cu}$, ρ_{Gr}, and ρ_{Cu} are the charge density of the total system, Cu slab, and graphene, respectively. The yellow and gray isosurfaces are plotted as values of ±0.0005 |e| Bohr^{-3} and represent charge accumulation and depletion, respectively. The magnified plot of the charge density difference shows the 2D cross-section passing through the uppermost Cu atom and the C atom above.

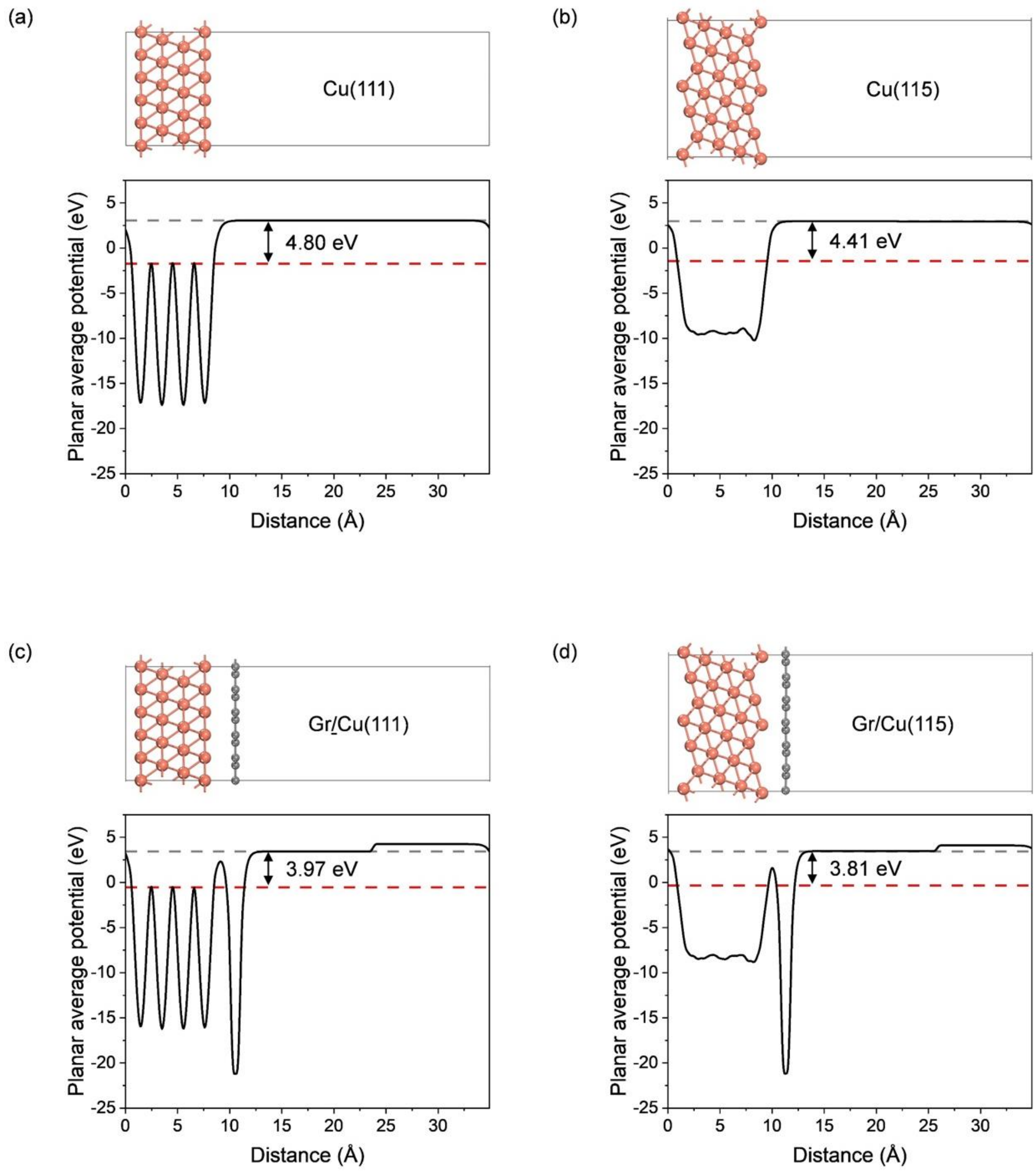

Figure S19. Planar average potential and calculated work functions for (a) Cu(111), (b) Cu(115), (c) Gr/Cu(111), and (d) Gr/Cu(115) surfaces. The red and gray dashed lines represent the Fermi level and vacuum level, respectively.

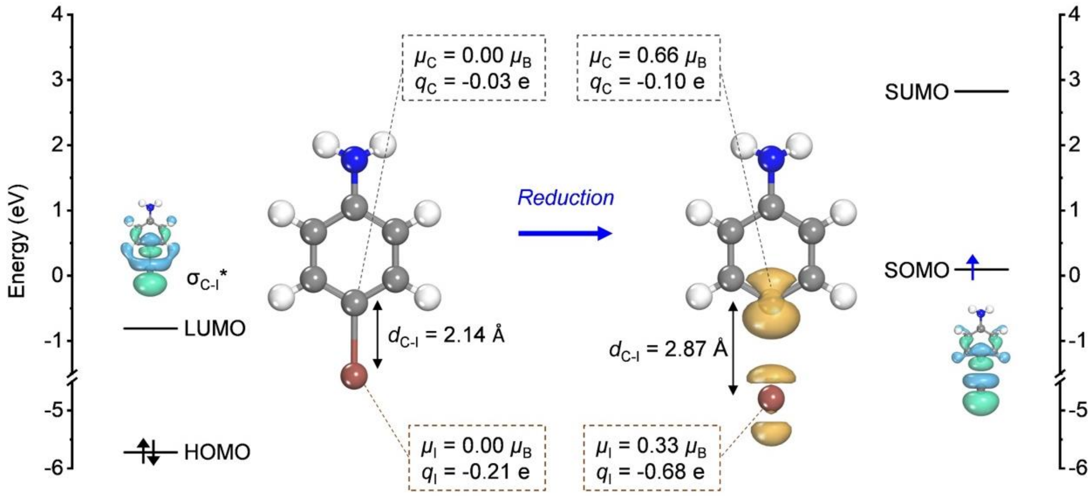

Figure S20. Optimized structure of neutral (left) and reduced (right) 4-iodoaniline with molecular orbital energy levels and spin density. The HOMO (LUMO) is the highest (lowest) occupied (unoccupied) molecular orbital and SOMO (SUMO) is the singly occupied (unoccupied) molecular orbital. $\sigma_{C\text{-}I}$* indicates that the LUMO is the antibonding orbital associated with the C-I bond of 4-iodoaniline. $d_{C\text{-}I}$, μ_C, q_C, μ_I, and q_I are the interatomic distance between iodine and carbon, magnetic moment of carbon, atomic charge of carbon, magnetic moment of iodine, and atomic charge of iodine, respectively. The yellow isosurface represents the spin density.

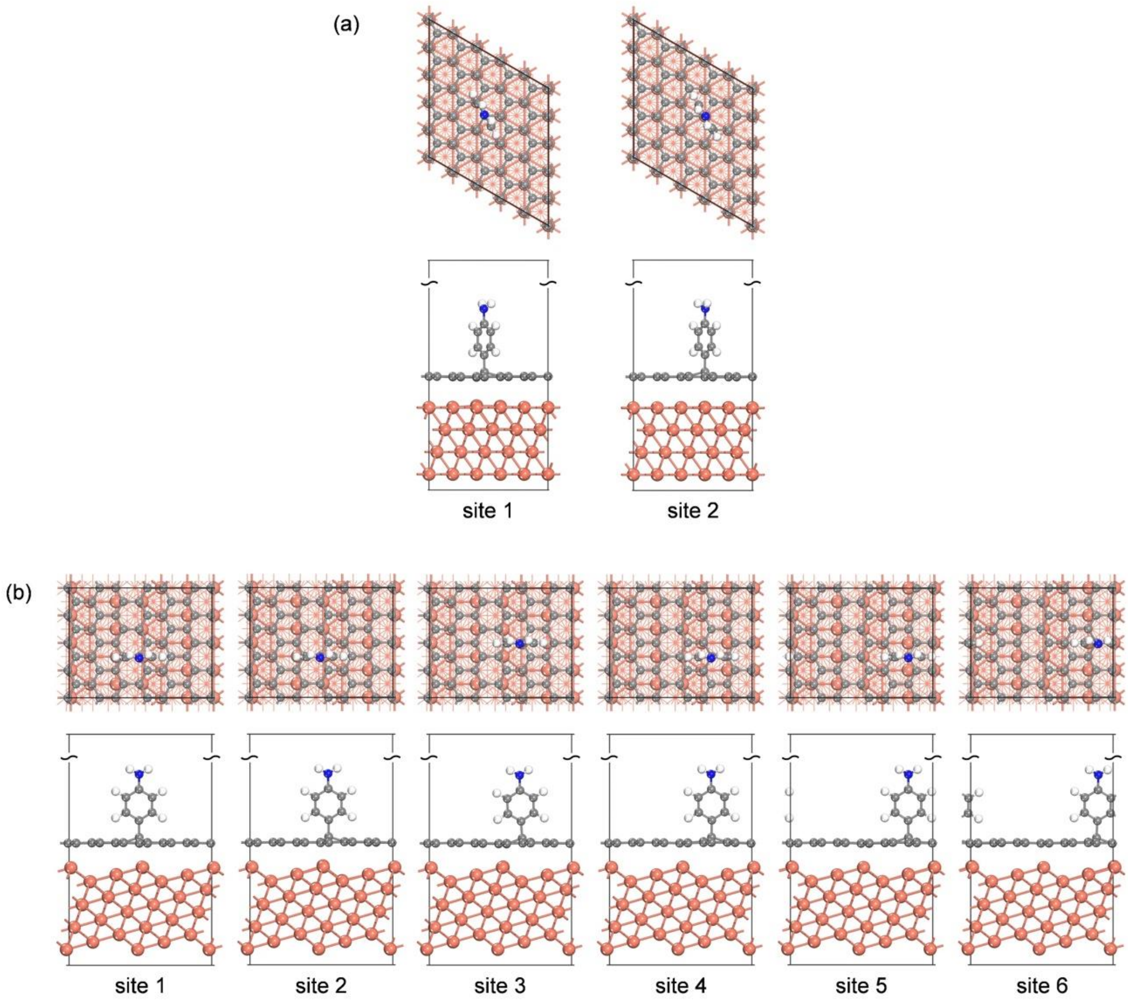

Figure S21. (a) Gr/Cu(111) and (b) Gr/Cu(115) slab models with aniline adsorbed at symmetrically inequivalent adsorption sites (top: top view, bottom: side view). In the top view, only the topmost Cu atomic layer is shown as a ball-and-stick model for clarity.

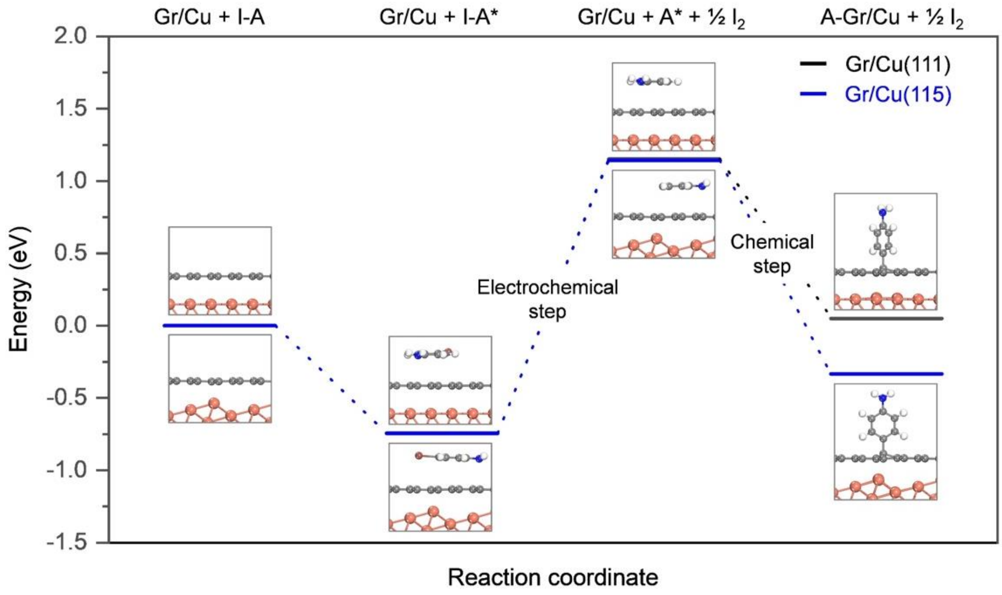

Figure S22. Energy diagram for the electrochemical functionalizattion of 4-iodoaniline on (black line) Gr/Cu(111) and (blue line) Gr/Cu(115) surfaces. I-A and A indicate 4-iodoanilie and aniline, respectively. The asterisk (*) represents the adsorbed state.

Supplementary References

[1] Kresse, G. & Furthmüller, J. (1996). Efficient iterative schemes for *ab initio* total-energy calculations using a plane-wave basis set, *Physical Review B*, 54(16), 11169.

[2] Kresse, G. & Joubert, D. (1999). From ultrasoft pseudopotentials to the projector augmented-wave method, *Physical Review B*, 59, 1758.

[3] Perdew, J. P., Burke, K., & Ernzerhof, M. (1996). Generalized Gradient Approximation Made Simple. *Physical Review Letters*, 77(18), 3865.

[4] Grimme, S. (2006). Semiempirical GGA-type density functional constructed with a long-range dispersion correction. *Journal of Computational Chemistry*, 27(15), 1787.

[5] Dassault Systèmes BIOVIA, Materials Studio, 2019, San Diego: Dassault Systèmes, 2019.

[6] Sun, H., Jin, Z., Yang, C., Akkermans, R. L. C., Robertson, S. H., Spenley, N. A., Miller S., & Todd, S. M. (2016). COMPASS II: extended coverage for polymer and drug-like molecule databases. *Journal of Molecular Modeling*, 22(2), 47.

[7] Ewald, P. P. (1921). Die Berechnung optischer und elektrostatischer Gitterpotentiale. a*nnalen der physik*, 369(3), 253.